




Large anisotropic magnetocaloric effect in all-sputtered epitaxial terbium thin films

Mohammed Salah El Hadri ^{1,*}, Vincent Polewczyk ², Yuxuan Xiao,¹ Stéphane Mangin ² and Eric Fullerton^{1,3}

¹Center for Memory and Recording Research, University of California, San Diego, La Jolla, California, 92093-0401, USA

²Institut Jean Lamour, UMR CNRS 7198, Université de Lorraine, Nancy 54000, France

³Department of Electrical and Computer Engineering, University of California, San Diego, 9500 Gilman Drive, La Jolla, California 92093-0407, USA



(Received 21 September 2020; revised 16 November 2020; accepted 23 November 2020; published 10 December 2020)

We present an experimental investigation of the magnetic and magnetocaloric properties of sputtered epitaxial and amorphous Tb thin films. We grew epitaxial Nb (50-nm)/Tb (100-nm) bilayer thin films on Al₂O₃(1120) substrate using DC magnetron sputtering at high temperature, with excellent crystalline quality of the hcp Tb(0001) layer. While the amorphous Tb thin film exhibits more isotropic magnetocaloric properties, we show that the epitaxial Tb thin film displays large anisotropic magnetocaloric properties, with a large maximum magnetic entropy change of 6.27 J kg⁻¹ K⁻¹ at the Néel temperature as well as a large relative cooling power of 225 J kg⁻¹ with a magnetic field change $\Delta H = 20$ kOe applied along the in-plane direction. These large and anisotropic magnetocaloric properties are much larger than those measured for the amorphous Tb thin film, or previously reported for Tb-based thin-film structures. Our findings highlight the opportunities for growing epitaxial rare-earth thin films using sputtering techniques and demonstrate the importance of crystallographic control on the magnetocaloric effect in Tb thin films.

DOI: [10.1103/PhysRevMaterials.4.124404](https://doi.org/10.1103/PhysRevMaterials.4.124404)

I. INTRODUCTION

Investigation of the magnetic refrigeration based on the magnetocaloric effect has attracted increasing experimental [1–4] and theoretical [5] interest over the last three decades due to the prospect of exploring novel magnetic refrigerants and achieving energy efficient and environmentally protective refrigeration technologies [6,7]. Since the discovery of the sub-room-temperature giant magnetocaloric effect (MCE) in a Gd₅(Si₂Ge₂) alloy by Pecharsky and Gschneidner [8], efforts have been directed towards exploring several material classes with giant magnetocaloric properties close to ambient conditions [9–19]. Among the rare-earth (RE) metals, Tb is one of the more interesting since it offers a large magnetic moment and has the advantage of combining the properties of a relatively high Curie temperature ($T_C = 220$ K) as well as a strong magnetic anisotropy unlike Gd [20–22]. Furthermore, bulk Tb displays a transition from the paramagnetic (PM) to the ferromagnetic (FM) phase via a basal-plane helical antiferromagnetic (HAFM) phase in the temperature interval from the Néel temperature $T_N = 230$ K to the Curie temperature $T_C = 220$ K [6,23,24]. Therefore, the magnetocaloric properties of bulk Tb have been the focus of increasing research interest, evidenced by many experimental [21,25,26] and theoretical investigations [27–30]. Initial experimental work by Nikitin and Tishin [21] has shown that bulk single-crystal Tb exhibits a large maximum magnetic entropy change ($-\Delta S_M^{\max}$) of 15.7 J kg⁻¹ K⁻¹ at $T_N = 230$ K and for a magnetic field change $\Delta H = 60.2$ kOe. Later, followup experiments investigated the magnetocaloric

properties of Tb-based bulk intermetallic compounds, such as single-crystalline Tb₂PbSi₃ [31] and Tb₅(Si_{0.5}Ge_{0.5})₄ [32] compounds, as well as polycrystalline Tb₃Co [33] and TbCoC₂ compounds [34].

In a similar vein, the role of nanostructuring on the magnetocaloric effect has also attracted recent experimental and theoretical interest [35–37], in an aim to obtain novel materials exhibiting unique magnetocaloric properties [35]. Indeed, recent studies of different classes of thin-film materials have revealed the critical role of size, strain, and interfacial effects in tailoring the magnetic properties to enhance the magnetocaloric properties [38–47], thus highlighting the potential of thin films for novel magnetocaloric applications [35]. Moreover, it has been demonstrated that reducing the dimensionality of Tb-based structures plays an important role in tailoring their magnetocaloric properties, as reported experimentally for Gd_{1-x}Tb_x heterostructure thin films [41,42] and Tb-doped Gd₂O₃ nanoparticles [48], and theoretically for single-crystal Tb thin films [28–30]. Nevertheless, growing high-quality epitaxial Tb thin films remains challenging from an application-minded point of view since advanced crystal growth techniques such as molecular beam epitaxy [49] and pulsed laser deposition [50] are generally required. On the other hand, the magnetron sputtering technique is more desirable for magnetocaloric applications, as it allows for easily scalable production; however, it can be difficult to achieve high-quality epitaxial films from sputtering. In this paper, we demonstrate the successful growth of a hcp-Tb(0001) thin film with excellent crystalline quality on a sapphire substrate simply using the sputtering technique, and present an experimental comparison of the magnetocaloric properties of sputtered epitaxial and amorphous Tb thin films.

*melhadri@ucsd.edu

II. SAMPLE FABRICATION

To elucidate the structural dependence of the magnetocaloric properties in Tb thin films, we investigated two different samples, epitaxial and amorphous 100-nm-thick Tb films grown on a Nb (50-nm) buffer layer. Each sample was deposited onto a $\text{Al}_2\text{O}_3(11\bar{2}0)$ substrate using a DC magnetron sputtering system with base pressure lower than 3×10^{-8} Torr. Prior to deposition, the sputtering targets of Nb and Tb were presputtered under deposition conditions for 15 min. For the epitaxial sample, the Nb and Tb layers were deposited at a substrate holder temperature of 400°C in an Ar gas atmosphere with a pressure fixed at 2.7 mTorr. The amorphous Tb film was deposited under identical condition but the substrate holder was at ambient temperature. During the sputtering deposition, both samples were grounded and in rotation to ensure good layer adhesion as well as homogeneous layer thickness. For the epitaxial sample, the Nb (50-nm) layer was sputter deposited in two steps: the first 5 nm of the Nb layer were deposited using at DC-sputtering power of 25 W, while the second 45 nm were deposited using a DC-sputtering power of 100 W. The first step at a DC-sputtering power of 25 W enables a relatively low sputtering rate of 0.13 $\text{\AA}/\text{s}$, which helps initiate a good epitaxial growth of Nb on $\text{Al}_2\text{O}_3(11\bar{2}0)$ substrate. For the amorphous sample, the entire Nb (50-nm) buffer layer was deposited using a DC-sputtering power of 100 W. Moreover, for both epitaxial and amorphous films, the 100-nm-thick Tb layer was then sputter deposited using a DC-sputtering power of 50 W. Later, each sample was capped with a 3-nm-thick MgO layer, grown by radio frequency (rf) sputtering at room temperature (RT) using a rf power of 150 W. The MgO capping layer helps prevent Tb oxidation. Sputtering rates for Nb at 25 and 100 W, Tb at 50 W, and MgO at 150 W were 0.13, 0.51, 0.67, and 0.13 $\text{\AA}/\text{s}$, respectively, as determined by performing low-angle x-ray reflectivity measurements on thicker calibration films.

The epitaxial growth of both Nb films on sapphire substrates and RE films on Nb films has been extensively studied in the literature [49,51–53]. It was previously reported that bcc Nb(110) grows epitaxially on $\text{Al}_2\text{O}_3(11\bar{2}0)$ substrate [51,52], and that hcp RE(0001) grows epitaxially on bcc Nb(110) following the Nishiyama-Wasserman orientation [49,53]. To investigate the epitaxial nature of the Nb/Tb bilayer thin films sputter deposited at 400°C , we performed specular θ - 2θ x-ray diffraction (XRD) measurements. As depicted in Fig. 1(a), the specular XRD pattern contains the $\text{Al}_2\text{O}_3(11\bar{2}0)$ substrate reflection, along with the bcc Nb(110) and hcp Tb(0002) reflections, thus demonstrating the epitaxial growth of the Nb/Tb bilayer film sputter deposited at 400°C . As shown in the Supplemental Material, Fig. S1 [54], the rocking curve across the Nb(110) and Tb(0002) peak gives full-width at half-maximum (FWHM) of 0.09° and 0.563° , respectively, indicating an excellent crystalline quality of both Nb(110) and hcp Tb(0001) layers. More importantly, the high-crystalline quality of our sputter-grown hcp Tb(0001), whose lattice structure is schematically represented in Fig. 1(b), is comparable to the one usually achieved with advanced crystal growth techniques such as molecular beam epitaxy [49] and pulsed laser deposition [50]. To further confirm the hexagonal structure of the epitaxial Tb layer, we measured in-plane XRD

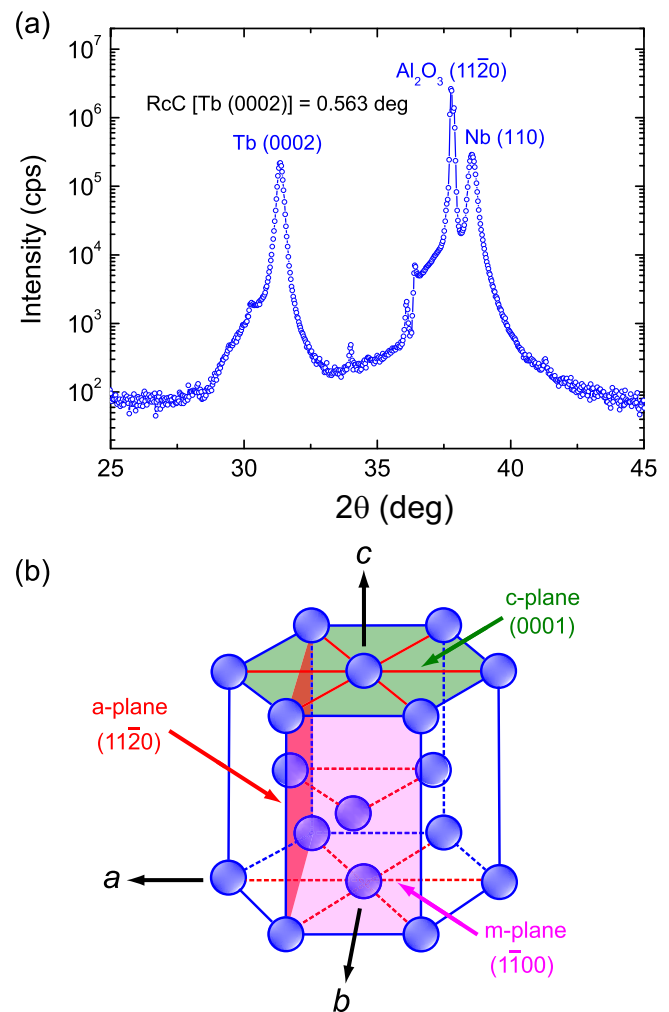


FIG. 1. (a) X-ray diffraction profile measured for the Nb (50-nm)/Tb (100-nm) bilayer sputtered on the $\text{Al}_2\text{O}_3(11\bar{2}0)$ substrate at 400°C , showing that the growth of the Tb epitaxial layer is oriented along the [0001] crystallographic direction. (b) Schematic representation of the Tb hcp lattice structure. The c , a , and b directions are parallel to the [0001], $[11\bar{2}0]$, and $[1\bar{1}00]$ crystallographic directions, respectively.

ϕ scans for the in-plane $(11\bar{2}0)$ and $(1\bar{1}00)$ Tb planes, along with the (0001) plan of the sapphire substrate (see Supplemental Material, Fig. S2 [54]). We first identified in-plane diffraction peaks at 50.72° and 28.44° for the Tb($11\bar{2}0$) and Tb($1\bar{1}00$) reflections, respectively, in agreement with data reported in Ref. [55]. One can see from Fig. S2 that well-defined sixfold symmetry peaks, with 60° separations in the ϕ axis, are clearly observed for both Tb($11\bar{2}0$) and Tb($1\bar{1}00$) reflections, thus confirming the hexagonal structure of the epitaxial Tb layer. Moreover, Fig. S2 shows that the respective in-plane peaks of Tb($11\bar{2}0$) and $\text{Al}_2\text{O}_3(0001)$ are separated by 5° in the ϕ axis, in agreement with previous studies [56]. We also performed specular θ - 2θ XRD measurements on the Nb/Tb bilayer thin films sputter deposited at RT. The specular XRD pattern contains no discernible reflections for Nb and Tb, thus confirming the amorphous, or at least strongly disordered, bilayer deposited at RT (see Supplemental Material, Fig. S3 [54]).

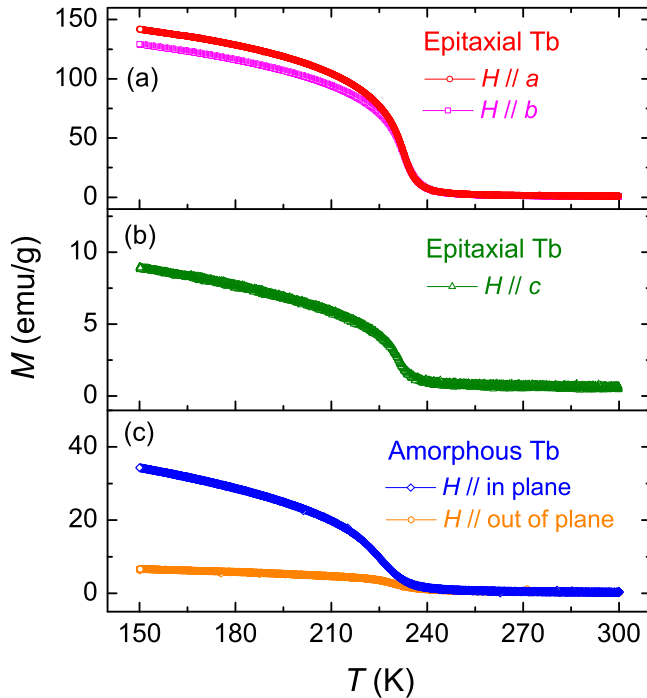


FIG. 2. Temperature dependence of magnetization measured for the studied epitaxial Tb film under an applied magnetic field of 500 Oe oriented along the (a) a , b , and (b) c directions. (c) Temperature dependence of magnetization measured for the studied amorphous Tb film under an applied magnetic field of 500 Oe oriented along out-of-plane and arbitrary in-plane directions.

III. MAGNETIC AND MAGNETOCALORIC MEASUREMENTS

To investigate the magnetic and magnetocaloric properties of the studied films, we performed both temperature- and magnetic-field-dependent measurements using a Quantum Design vibrating sample magnetometer system. For all the magnetic measurements, we removed the diamagnetic signal coming from the substrate by subtracting the measurements performed on a reference $\text{Al}_2\text{O}_3(11\bar{2}0)$ substrate under the same conditions from each data set. We first measured the temperature dependence of magnetization for the epitaxial Tb film under an applied magnetic field of 500 Oe oriented along the three principal crystallographic directions, namely, the a , b , and c directions, as depicted in Fig. 2. Note that the unit emu/g is used to represent the magnetization of Tb. Knowing the volume of the Tb film ($100 \text{ nm} \times 5 \text{ mm} \times 5 \text{ mm}$), the mass of the latter was calculated using the Tb density value of 8.23 g/cm^3 from Ref. [57]. Since the applied magnetic field of 500 Oe is much larger than the maximum critical field of Tb $H_{cr}^{\text{max}} = 190 \text{ Oe}$ [58], the basal-plane HAFM structure of Tb in the temperature interval between T_N and T_C is expected to be destroyed, and a direct paramagnetic to ferromagnetic phase transition is expected to take place at T_N [6].

One can see from Figs. 2(a) and 2(b) that a broad paramagnetic to ferromagnetic phase transition is observed at T_N for the epitaxial Tb film. By determining the minimum of the derivative of magnetization with respect to T , we found

a T_N value of 232 K for the epitaxial Tb film, in agreement with previous studies on bulk single-crystal Tb [6,23,24]. Furthermore, Figs. 2(a) and 2(b) show that the magnetization change at the phase transition with magnetic fields oriented along the in-plane a and b directions is significantly enhanced compared to the field being along the out-of-plane c direction. This implies a strong in-plane magnetic anisotropy for the epitaxial Tb film and an easy axis lying in plane, which is consistent with the literature [6,25]. Moreover, one can see from Fig. 2(a) that the magnetization curves measured along the in-plane a and b directions are very similar, however, with a slightly weaker magnetic anisotropy along the in-plane a direction at the ferromagnetic phase. Surprisingly, this finding is at the opposite of what was reported for bulk single-crystal Tb, where the magnetic anisotropy was slightly weaker along the b direction at the ferromagnetic phase [22]. This discrepancy might be ascribed to the thin-film effects, such as strains and dislocations, in the studied epitaxial Tb film.

We further measured the temperature dependence of magnetization for the studied amorphous Tb film under an applied magnetic field of 500 Oe oriented in plane and out of plane. As shown in Fig. 2(c), a broad paramagnetic to ferromagnetic phase transition is also observed at T_N for the amorphous Tb film with an easy axis of magnetization lying in plane. Nevertheless, the magnetization change measured for the amorphous Tb film is four times lower compared to the one observed for the epitaxial Tb film along the in-plane directions. This finding could be explained by the disordered nature of the amorphous Tb layer, which leads to an increased defect density and therefore to a lower magnetization. Surface roughness and grain microstructure effects might also explain the low magnetization of the amorphous Tb layer, in agreement with previous studies [59–62]. Moreover, we found a T_N value of 227 K for the amorphous Tb film from the minimum of the derivative of magnetization with respect to T . Hence, the slight difference between the T_N values of both epitaxial and amorphous Tb films is attributed to their different crystal structures. More importantly, the difference in magnetization change at the phase transition between the in-plane and out-of-plane directions measured for the amorphous Tb film is three times smaller compared to the one observed for the epitaxial Tb film, indicating that the latter exhibits a much stronger in-plane magnetic anisotropy.

To determine the saturation magnetization and coercive field as a function of the magnetic ordering, we performed temperature-dependent hysteresis loop measurements where the magnetic field is applied in plane for both the amorphous and epitaxial Tb films. Figure 3(a) shows that both studied films exhibit a square hysteresis at $T = 150 \text{ K}$ with the magnetic field oriented in plane, thus confirming that both films show a ferromagnetic order below T_N with in-plane magnetic anisotropy. We measured a saturation magnetization M_S of 183 emu/g for the epitaxial Tb film at $T = 150 \text{ K}$, which is smaller than the M_S of 260 emu/g previously reported for bulk single-crystal Tb [22]. On the other hand, we measured a much smaller M_S of 68 emu/g for the amorphous Tb film at $T = 150 \text{ K}$, which might be attributed the increased defect density in the amorphous film. Moreover, coercive field H_C of 852 and 2620 Oe are measured at $T = 150 \text{ K}$ for the

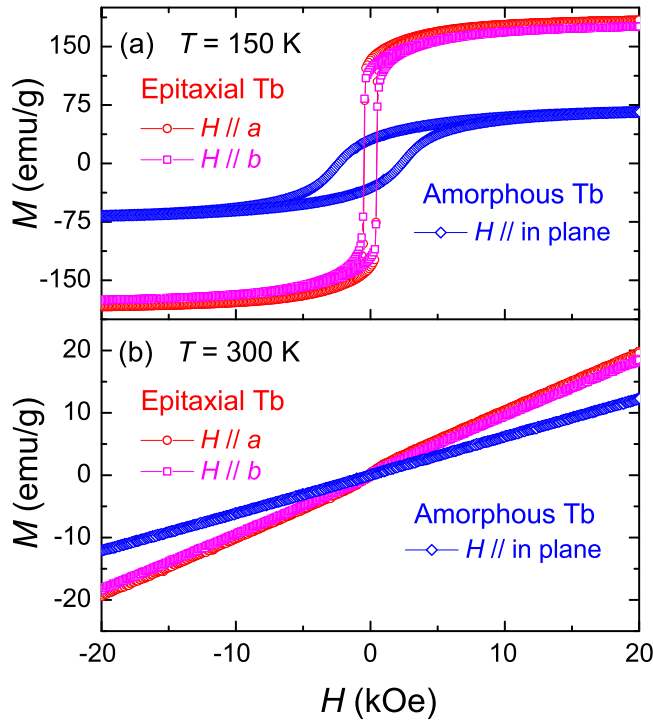


FIG. 3. In-plane magnetic hysteresis loops for the epitaxial Tb film (magnetic field oriented along the a and b axes and the amorphous films). The magnetic hysteresis loops are measured at 150 K in (a) and 300 K in (b).

epitaxial and amorphous Tb films, respectively, which is also in agreement with an increased defect density in the amorphous film. To confirm the paramagnetic phase at $T = 300$ K, we also performed RT hysteresis loop measurements for both Tb films. One can see from Fig. 3(c) that the RT hysteresis loops are linear, which is a signature of paramagnetic behavior. The hysteresis loops measured for the epitaxial and amorphous Tb films along the out-of-plane direction can be found in the Supplemental Material, Fig. S4 [54].

We further studied the MCE in the studied epitaxial and amorphous Tb films by measuring the magnetization isotherms for temperatures ranging from 150 to 300 K in steps of $\Delta T = 5$ K. The applied magnetic field is swept from 0 to $\Delta H = 20$ kOe using a moderate sweeping rate of 100 Oe/s, and is oriented along the in-plane and out-of-plane directions. The example magnetization isotherms measured for the epitaxial and amorphous Tb films under the applied magnetic field oriented along the a and in-plane directions, respectively, are shown in Fig. 4. One can see from Fig. 4 that the magnetization curves with T below T_N exhibit a nonlinear behavior and a tendency to saturate under the applied magnetic field, which is a signature of ferromagnetic behavior. The magnetization isotherms measured for the epitaxial Tb film along the b and c directions, and for the amorphous Tb film along the out-of-plane direction can be found in the Supplemental Material, Fig. S5 [54].

Based on the magnetization isotherms, the magnetic entropy change $-\Delta S_M$ due to an applied magnetic field from 0 to ΔH is then obtained using the Maxwell relation, which can be approximated for data taken a discrete field and temperature

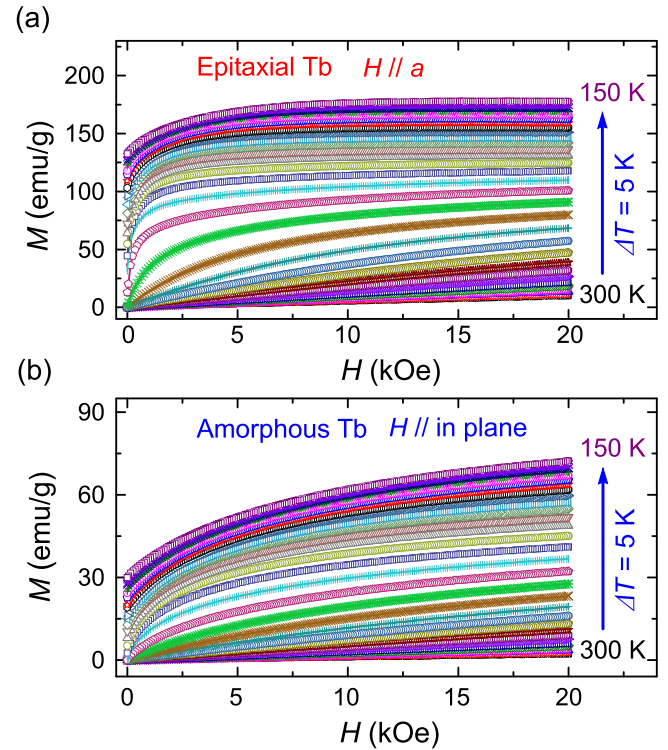


FIG. 4. (a) [respectively (b)] Magnetization isotherms of the studied epitaxial (respectively amorphous) Tb film as function of the applied magnetic field from 0 to 20 kOe with a sweeping rate of 100 Oe/s. The applied magnetic field is oriented along the a direction and an arbitrary in-plane direction for the studied epitaxial and amorphous Tb films, respectively.

intervals as [39]

$$\Delta S_M(T, \Delta H) = \mu_0 \sum_j \frac{M_{i+1}(T_{i+1}, H_j) - M_i(T_i, H_j)}{T_{i+1} - T_i} \Delta H_j, \quad (1)$$

where μ_0 is the permeability of free space, $T_{i+1} = T + \frac{\Delta T}{2}$, and $T_i = T - \frac{\Delta T}{2}$. Two major sources of uncertainty can influence the accuracy of the calculated magnetic entropy change values, namely, the magnetic measurement itself and the film thickness determination. Note that we used an oscillation amplitude of 2 mm for all the magnetic measurements. Since the length of the sample is 5 mm, the typical uncertainty on the magnetic measurement itself is about 6%, as previously reported in Ref. [63]. On the other hand, we have carefully calibrated the deposition of Tb at room temperature and 400 °C by performing low-angle x-ray reflectivity measurements. However, the typical error on the Tb calibration, and therefore on the Tb layer thickness, is about 5%. By taking into account both sources of uncertainty, we estimate a total error of about 11% on the calculated magnetic entropy change values. Figure 5 shows the magnetic entropy change calculated for both epitaxial and amorphous Tb films as a function of temperature, under an applied field change interval of $\Delta H = 20$ kOe oriented along the in-plane and out-plane directions.

One can see from Fig. 5 that the epitaxial Tb film exhibits large anisotropic magnetocaloric properties. A large magnetic

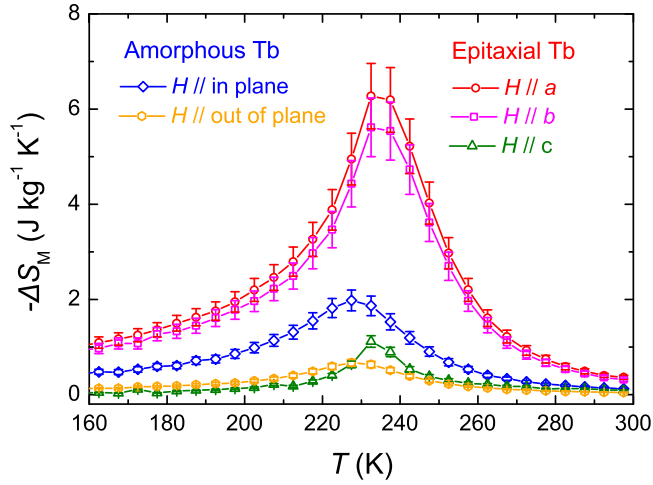


FIG. 5. Temperature dependence of the magnetic entropy change $-\Delta S_M$ measured for the studied epitaxial and amorphous Tb films under an applied field change interval of $\Delta H = 20$ kOe.

entropy change peak is measured under an applied magnetic field oriented along the in-plane a and b directions, with a large maximum magnetic entropy change ($-\Delta S_M^{\max}$) of 6.27 ± 0.69 and 5.61 ± 0.61 $\text{J kg}^{-1} \text{K}^{-1}$, respectively, and at a peak temperature $T_{\max}^S = T_N = 232$ K. These values are slightly lower than those reported for single-crystal bulk Tb [9,21,26], but are much larger than those reported for Tb-based thin-film structures such as $[\text{Gd}_x\text{Tb}_{1-x}/\text{Ti}]$ multilayers [41] and $\text{Gd}_x\text{Tb}_{1-x}$ alloy films [42] (see Table I). Note that no MCE anomalies were measured for the studied epitaxial Tb film near $T_C = 220$ K, thus confirming the destruction of the basal-plane HAFM structure between T_N and T_C , as well as the direct paramagnetic to ferromagnetic phase transition at T_N . On the other hand, the $-\Delta S_M$ peak measured for the epitaxial Tb film under an applied magnetic field oriented in the out-of-plane c direction is drastically damped out and exhibits a much smaller $-\Delta S_M^{\max}$ value of 1.11 ± 0.12 $\text{J kg}^{-1} \text{K}^{-1}$ at $T_{\max}^S = T_N = 232$ K. Such a small $-\Delta S_M^{\max}$ value is roughly 5.6 times smaller than the one measured with a magnetic field oriented along the a direction, which demonstrates the

strongly anisotropic MCE in the studied epitaxial Tb films. Figure 5 shows that the amorphous Tb film which, in contrast to the epitaxial Tb film, exhibits a much lower magnetic entropy change under an applied magnetic field oriented along the in-plane direction, with a maximum $-\Delta S_M^{\max}$ of 1.98 ± 0.22 $\text{J kg}^{-1} \text{K}^{-1}$ at a peak temperature $T_{\max}^S = T_N = 227$ K, which is three times smaller than the one measured for the epitaxial Tb film with magnetic fields oriented along the a direction. Finally, the amorphous Tb film shows a $-\Delta S_M^{\max}$ value of 0.67 ± 0.07 $\text{J kg}^{-1} \text{K}^{-1}$ with magnetic fields oriented in the out-of-plane direction, which is roughly three times smaller than the one measured for the amorphous Tb film in-plane direction. These findings reveal the large and anisotropic nature of the MCE in the epitaxial Tb thin film, in contrast to the one in amorphous Tb thin film. Finally, we measured the relative cooling power (RCP), which is an important parameter quantifying the efficiency in terms of heat transfer between the cold and hot ends in an ideal thermodynamic cycle. The RCP can be calculated using the following equation:

$$\text{RCP} = -\Delta S_M^{\max} \times \delta T_{\text{FWHM}}, \quad (2)$$

where $-\Delta S_M^{\max}$ is the maximum magnetic entropy change and δT_{FWHM} is the full-width at half-maximum of the magnetic entropy change curve. Hence, we found large RCP values of 225, 199, and 18 J kg^{-1} for the epitaxial Tb film at 20 kOe applied magnetic field along the in-plane a , b , and c directions, respectively. These findings further confirm the anisotropic nature of the MCE in the studied epitaxial Tb film. Moreover, these RCP values measured for the a and b directions are significantly larger than those reported for other Tb-based thin-film structures [42] (see Table I). We have also found lower RCP values of 86 and 25 J kg^{-1} for the amorphous Tb film with 20 kOe applied magnetic field along the in-plane and out-of-plane directions, respectively, thus confirming the absence of anisotropic and large magnetocaloric properties in the studied amorphous Tb film.

IV. CONCLUSION

In conclusion, we have experimentally investigated the magnetic and magnetocaloric properties of sputtered epitaxial

TABLE I. Main magnetocaloric properties of the studied epitaxial and amorphous Tb thin films and of other Tb-based materials reported in the literature, such as single-crystal bulk Tb [9,21,26] and Tb-based thin-film structures [41,42].

Materials	T_{\max}^S (K)	$-\Delta S_M^{\max}$ ($\text{J kg}^{-1} \text{K}^{-1}$)	ΔH (kOe)	H direction	References
Single-crystal bulk Tb	230	3.8	12	$H \parallel a$	[9]
	232	9	20		[26]
	230	15.7	60.2		[21]
Epitaxial Tb (100 nm) film	232	6.27 ± 0.69	20	$H \parallel a$	This work
	232	5.61 ± 0.61	20	$H \parallel b$	This work
	232	1.11 ± 0.12	20	$H \parallel c$	This work
Amorphous Tb (100 nm) film	227	1.98 ± 0.22	20	$H \parallel \text{IP}$	This work
	227	0.67 ± 0.07	20	$H \parallel \text{OOP}$	This work
Amorphous $[\text{Gd}_{90}\text{Tb}_{10}/\text{Ti}]_{60}$ multilayers	83	9	70		[41]
Amorphous $\text{Tb}_{80}\text{Gd}_{20}$ (100 nm) film	232	2.76	20	$H \parallel \text{OOP}$	[42]

and amorphous Tb thin films. We successfully grew epitaxial hcp Tb(0001) layer on Al₂O₃(11 $\bar{2}$ 0) substrate with excellent crystalline quality. We showed via magnetometry measurements that the epitaxial Tb thin film displays large and anisotropic magnetocaloric properties, with a large $-\Delta S_M^{\max}$ of 6.27 J kg⁻¹ K⁻¹ near $T_N = 232$ K as well as a large RCP of 225 J kg⁻¹ with a magnetic field change of 20 kOe applied along the in-plane *a* direction. On the other hand, we demonstrated that the amorphous Tb thin film displays lower and more isotropic magnetocaloric properties, with $-\Delta S_M^{\max}$ of 1.98 J kg⁻¹ K⁻¹ near $T_N = 227$ K and RCP of 86 J kg⁻¹ with a magnetic field change of 20 kOe applied along the in-plane direction. Our findings highlight the opportunities for growing

epitaxial rare-earth thin films using sputtering techniques and, more importantly, show the importance of crystallographic control on the magnetocaloric effect in Tb thin films.

ACKNOWLEDGMENTS

This research was supported by the research programs of the U. S. Department of Energy (DOE), Office of Basic Energy Sciences Award No. DE-SC0003678. The authors would like to thank R. Descoteaux from CMRR for technical assistance.

M.S.E.H. and V.P. contributed equally to this work.

The authors declare no competing financial interests.

-
- [1] V. K. Pecharsky and K. A. Gschneider, Jr., *J. Magn. Magn. Mater.* **200**, 44 (1999).
- [2] K. A. Gschneider, Jr. and V. K. Pecharsky, *Annu. Rev. Mater. Sci.* **30**, 387 (2000).
- [3] K. A. Gschneider, Jr., V. K. Pecharsky, and A. O. Tsokol, *Rep. Prog. Phys.* **68**, 1479 (2005).
- [4] M.-H. Phan and S.-C. Yu, *J. Magn. Magn. Mater.* **308**, 325 (2007).
- [5] N. A. de Oliveira and P. J. von Ranke, *Phys. Rep.* **489**, 89 (2010).
- [6] A. M. Tishin and Y. I. Spichkin, *The Magnetocaloric Effect and Its Applications* (Institute of Physics, Bristol, 2003).
- [7] J. Romero Gómez, R. Ferreira Garcia, A. De Miguel Catoira, and M. Romero Gómez, *Renewable Sustainable Energy Rev.* **17**, 74 (2013).
- [8] V. K. Pecharsky and K. A. Gschneider, Jr., *Phys. Rev. Lett.* **78**, 4494 (1997).
- [9] S. Y. Dan'kov, A. M. Tishin, V. K. Pecharsky, and K. A. Gschneider, Jr., *Phys. Rev. B* **57**, 3478 (1998).
- [10] A. O. Pecharsky, K. A. Gschneider, Jr., and V. K. Pecharsky, *J. Appl. Phys.* **93**, 4722 (2003).
- [11] T. Krenke, E. Duman, M. Acet, E. F. Wassermann, X. Moya, L. Mañosa, and A. Planes, *Nat. Mater.* **4**, 450 (2005).
- [12] J. Liu, T. Gottschall, K. P. Skokov, J. D. Moore, and O. Gutfleisch, *Nat. Mater.* **11**, 620 (2012).
- [13] H. Wada and Y. Tanabe, *Appl. Phys. Lett.* **79**, 3302 (2001).
- [14] O. Tegus, E. Brück, K. H. J. Buschow, and F. R. de Boer, *Nature (London)* **415**, 150 (2002).
- [15] A. Yan, K.-H. Müller, L. Schultz, and O. Gutfleisch, *J. Appl. Phys.* **99**, 08K903 (2006).
- [16] F.-X. Hu, B.-G. Shen, J.-R. Sun, Z.-H. Cheng, G.-H. Rao, and X.-X. Zhang, *Appl. Phys. Lett.* **78**, 3675 (2001).
- [17] R. D. McMichael, J. J. Ritter, and R. D. Shull, *J. Appl. Phys.* **73**, 6946 (1993).
- [18] M.-H. Phan, S.-C. Yu, and N. H. Hur, *Appl. Phys. Lett.* **86**, 072504 (2005).
- [19] A. Midya, S. N. Das, P. Mandal, S. Pandya, and V. Ganesan, *Phys. Rev. B* **84**, 235127 (2011).
- [20] S. A. Nikitin, A. M. Tishin, and S. E. Bykhover, *Phys. Status Solidi A* **114**, 99 (1989).
- [21] S. A. Nikitin and A. M. Tishin, *Pisma v Zh. Tekh. Fiz.* **14**, 735 (1988) [*Sov. Tech. Phys. Lett.* **14**, 327 (1988)].
- [22] Ed. R. J. Elliott, *Magnetic Properties of the Rare-Earth Metals* (Plenum, New York, 1972).
- [23] C. Dufour, K. Dumesnil, A. Mougin, Ph. Mangin, G. Marchal, and M. Hennion, *J. Phys.: Condens. Matter* **9**, L131 (1997).
- [24] C. Dufour, K. Dumesnil, A. Mougin, Ph. Mangin, and M. Hennion, *J. Phys.: Condens. Matter* **11**, L497 (1999).
- [25] S. Y. Dan'kov, Yu. I. Spichkin, and A. M. Tishin, *J. Magn. Magn. Mater.* **152**, 208 (1996).
- [26] A. S. Chernyshov, A. M. Tishin, K. A. Gschneider, Jr., V. K. Pecharsky, and A. O. Pecharsky (unpublished).
- [27] A. M. Tishin, *Magnetic, Magnetothermal and Magnetoelastic Properties of Heavy Rare Earth Metals and their Alloys in the Region of Magnetic Phase Transitions*, Ph.D. thesis, Moscow State University, 1994.
- [28] D. H. A. L. Anselmo, V. D. Mello, and M. S. Vasconcelos, *Simulation of the Magnetocaloric Effect in Tb Nanofilms*, *AIP Conf. Proc.* **1590**, 79 (2014).
- [29] V. D. Mello, D. H. A. L. Anselmo, M. S. Vasconcelos, and N. S. Almeida, *Solid State Commun.* **268**, 56 (2017).
- [30] R. R. Gimaev, V. I. Zverev, and V. D. Mello, *J. Magn. Magn. Mater.* **505**, 166781 (2020).
- [31] S. Majumdar, E. V. Sampathkumaran, P. L. Paulose, H. Bitterlich, W. Löser, and G. Behr, *Phys. Rev. B* **62**, 14207 (2000).
- [32] L. Morellon, C. Magen, P. A. Algarabel, M. R. Ibarra, and C. Ritter, *Appl. Phys. Lett.* **79**, 1318 (2001).
- [33] B. Li, J. Du, W. J. Ren, W. J. Hu, Q. Zhang, D. Li, and Z. D. Zhang, *Appl. Phys. Lett.* **92**, 242504 (2008).
- [34] B. Li, W. J. Hu, X. G. Liu, F. Yang, W. J. Ren, X. G. Zhao, and Z. D. Zhang, *Appl. Phys. Lett.* **92**, 242508 (2008).
- [35] C. W. Miller, D. D. Belyea, and B. J. Kirby, *J. Vac. Sci. Technol. A* **32**, 040802 (2014).
- [36] V. D. Mello, A. L. Dantas, and A. S. Carriço, *Solid State Commun.* **140**, 447 (2006).
- [37] F. C. Medeiros Filho, V. D. Mello, A. L. Dantas, F. H. S. Sales, and A. S. Carriço, *J. Appl. Phys.* **109**, 07A914 (2011).
- [38] G. Z. Gadioli, F. P. Rouxinol, R. V. Gelamo, A. O. dos Santos, L. P. Cardoso, and M. A. Bica de Moraes, *J. Appl. Phys.* **103**, 093916 (2008).
- [39] C. W. Miller, D. V. Williams, N. S. Bingham, and H. Srikanth, *J. Appl. Phys.* **107**, 09A903 (2010).

- [40] S. P. Mathew and S. N. Kaul, *Appl. Phys. Lett.* **98**, 172505 (2011).
- [41] A. V. Svalov, V. O. Vas'kovskiy, J. M. Barandiaran, K. G. Balymov, I. Orue, and G. V. Kurlyandskaya, *Phys. Status Solidi A* **208**, 2273 (2011).
- [42] C. H. Lambert, M. S. El Hadri, M. Hamedoun, A. Benyoussef, O. Mounkachi, and S. Mangin, *J. Magn. Magn. Mater.* **443**, 1 (2017).
- [43] M. Tadout, C.-H. Lambert, M. S. El Hadri, O. Mounkachi, A. Benyoussef, M. Hamedoun, M. Benaïssa, and S. Mangin, *J. Appl. Phys.* **123**, 053902 (2018).
- [44] M. Tadout, C.-H. Lambert, M. S. El Hadri, A. Benyoussef, M. Hamedoun, M. Benaïssa, O. Mounkachi, and S. Mangin, *Crystals* **9**, 278 (2019).
- [45] V. Recarte, J. I. Pérez-Landazábal, V. Sánchez-Alárcos, V. A. Chernenko, and M. Ohtsuka, *Appl. Phys. Lett.* **95**, 141908 (2009).
- [46] Q. Zhang, S. Thota, F. Guillou, P. Padhan, V. Hardy, A. Wahl, and W. Prellier, *J. Phys.: Condens. Matter* **23**, 052201 (2011).
- [47] P. Lampen, N. S. Bingham, M. H. Phan, H. Kim, M. Osofsky, A. Pique, T. L. Phan, S. C. Yu, and H. Srikanth, *Appl. Phys. Lett.* **102**, 062414 (2013).
- [48] S. Hazarika, D. Mohanta, and R. Nirmala, *Phys. B (Amsterdam)* **570**, 324 (2019).
- [49] J. Kwo, M. Hong, and S. Nakahara, *Appl. Phys. Lett.* **49**, 319 (1986).
- [50] N. Kumar, N. G. Kim, Y. A. Park, N. Hur, J. H. Jung, K. J. Han, and K. J. Yee, *Thin Solid Films* **516**, 7753 (2008).
- [51] G. Song, A. Remhof, K. Theis-Bröhl, and H. Zabel, *Phys. Rev. Lett.* **79**, 5062 (1997).
- [52] A. R. Wildes, J. Mayer, and K. Theis-Bröhl, *Thin Solid Films* **401**, 7 (2001).
- [53] S. M. Paik and I. K. Schuller, *Phys. Rev. Lett.* **64**, 1923 (1990).
- [54] See Supplemental Material at <http://link.aps.org/supplemental/10.1103/PhysRevMaterials.4.124404> for rocking curves measured across the Nb(110) and Tb(0001) Bragg peak, XRD ϕ scans measured for the in-plane (11 $\bar{2}$ 0) and (1 $\bar{1}$ 00) Tb planes, XRD profile measured for the Nb (50-nm)/Tb (100-nm) bilayer sputtered on the Al₂O₃(11 $\bar{2}$ 0) substrate at RT, magnetic hysteresis loops measured for the epitaxial and amorphous Tb films under an applied magnetic field oriented along the out-of-plane direction, and magnetization isotherms of the epitaxial (respectively amorphous) Tb film under an applied magnetic field oriented along the *b* and *c* (respectively out-of-plane) directions.
- [55] P. Kristin, Materials Data on Tb (SG:194) by Materials Project, [United States](https://materialsproject.org/materials/194) (2016).
- [56] K. Dumesnil, Couplage magnétique et Effets magnétostrictifs dans des films épitaxiés et superréseaux à base de Terres Rares, Ph.D. thesis, Institut National Polytechnique de Lorraine, 1995.
- [57] RSC, Terbium: The Royal Society of Chemistry **2020**, <https://www.rsc.org/periodic-table/element/65/terbium>.
- [58] S. E. Bykhover, S. A. Nikitin, Y. I. Spichkin, A. M. Tishin, and Z. S. Umkhaeva, *Zh. Eksp. i Teor. Fiz.* **97**, 1974 (1990) [*Sov. Phys.-JETP* **70**, 1121 (1990)].
- [59] M. Li, G.-C. Wang, and H.-G. Min, *J. Appl. Phys.* **83**, 5313 (1998).
- [60] J. Swerts, S. Vandezande, K. Temst, and C. Van Haesendonck, *Solid. State. Commun.* **131**, 359 (2004).
- [61] M. S. Pierce, C. R. Buechler, L. B. Sorensen, S. D. Kevan, E. A. Jagla, J. M. Deutsch, T. Mai, O. Narayan, J. E. Davies, Kai Liu, G. T. Zimanyi, H. G. Katzgraber, O. Hellwig, E. E. Fullerton, P. Fischer, and J. B. Kortright, *Phys. Rev. B.* **75**, 144406 (2007).
- [62] V. Polewczyk, G. Vinai, F. Motti, S. Santhosh, S. Benedetti, G. Rossi, and P. Torelli, *J. Magn. Magn. Mater.* **515**, 167257 (2020).
- [63] Quantum Design, Vibrating sample magnetometer (VSM) option user's manual (2011).